7

Electrochemical CO_2 reduction to formic acid on $Pd_{70}Pt_{30}$ nanoparticles on different supports

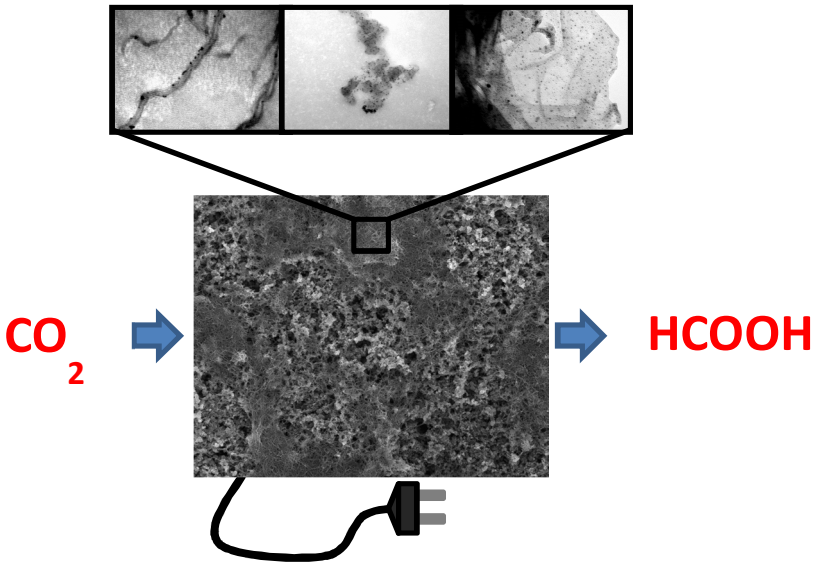

The contents of this chapter are being prepared for publication as: R. Kortlever, T.J.P. Hersbach, M. Koeman, M. Mulder, P. Bouwman and M.T.M. Koper, *in preparation*.

Abstract The electrochemical reduction of CO_2 to valuable products has gained interest lately, since it could close the anthropogenic carbon cycle. The production of formic acid is especially relevant, since formic acid can be used as a fine chemical and fuel. Here, we test $Pd_{70}Pt_{30}$ nanoparticles, which have been shown suitable for selective and efficient formic acid production, on different support materials to study the effect of the support on the efficiency of formic acid production. A clear support effect can be seen for both the electro-oxidation of formic acid and the reduction of CO_2 to formic acid on these catalyst. While Vulcan XC-72 supported nanoparticles show a maximum efficiency of 92% after 30 minutes of electrolysis at -0.4 V vs. RHE, nanoparticles on a multi-walled carbon nanotube support show a maximum efficiency of close to 100% after 30 minutes of electrolysis at -0.2 V vs. RHE.

7.1 Introduction

The electrochemical reduction of CO_2 has become a widely studied reaction, since it can potentially close the anthropogenic carbon cycle and thus could recycle atmospheric CO_2 into useful chemicals and fuels.[1-4] The CO_2 reduction reaction can yield multiple products, ranging from 2-electron transfer products such as CO and formic acid to multi-electron transfer products such as hydrocarbons and alcohols.[1,5,6] Formic acid and formate are products of special interest since they can be used as fine chemicals in multiple applications or serve directly as a fuel in direct formic acid fuel cells (DFAFCs).[7,8]

At present there are still major issues that need to be resolved before the electrochemical reduction of CO_2 becomes feasible. The main problems that are holding back the implementation of CO_2 reduction are the poor product selectivities and faradaic efficiencies, that are mainly caused by competition with the hydrogen evolution reaction (HER).[9] Furthermore, the high overpotentials that are needed to obtain products, as a result of inappropriate adsorption energies of reaction intermediates, decrease the energy storage efficiency.[10,11] However, recent developments in the field of CO_2 reduction to CO and formic acid have shown that the faradaic efficiency toward these products can be increased significantly, while simultaneously lowering the overpotentials for the reactions.[12-15]

In Chapter 5, we have reported the synthesis of a series of $Pd_xPt_{(100-x)}$/C nanoparticles and tested their electrocatalytic properties for the reduction of CO_2 to formic acid.[14] These nanoparticles display a very low onset potential for formic acid production of 0 V vs. RHE, which approaches the theoretical equilibrium potential of 0.02 V vs. RHE for this reaction. We showed that the optimal composition of $Pd_{70}Pt_{30}$/C gave a faradaic efficiency of 88% toward formic acid at -0.4 V vs. RHE at average current density of ~5 mA/cm^2, while avoiding strong deactivation as seen previously with Pd-based catalysts.[16] Furthermore, since this catalyst was designed from the reversible catalyst principle it is also active for reverse formic acid oxidation. Therefore, this catalyst has additional value for energy storage applications.

In this Chapter we will explore different possibilities to increase the applicability of the $Pd_{70}Pt_{30}$ nanoparticulate catalysts by changing the catalyst support, which is known to be an important parameter for the catalytic properties but is rarely studied in electrocatalytic CO_2 reduction.[17] We show that for both formic acid oxidation as CO_2 reduction a clear support effect can be seen for these catalysts.

7.2 Experimental

7.2.1 Materials

Cylindrical pyrolitic graphite electrodes, purchased at Carbone-Lorraine, with diameters of 5 mm and 10 mm, with a back contact to a platinum wire were used as working electrodes. Prior to every experiment the working electrodes were polished mechanically to a mirrorlike finish using P2500 sandpaper. After this, the electrodes were sonicated in ultra-pure water.

Electrolytes were prepared from ultra-pure water (Millipore MilliQ gradient A10 system, 18 mΩ cm) and high purity reagents (Merck Suprapur, Sigma Aldrich TraceSelect). Before each experiment the electrolytes were first purged with Argon (Air Products, 5.7) for 15 minutes to remove air from the solution. In

the case of CO_2 reduction experiments the electrolyte was subsequently purged with CO_2 (Linde, 4.5) for at least 30 minutes to saturate the solution.

7.2.2 Preparation and characterization of $Pd_{70}Pt_{30}$ nanoparticles on different supports

26.25 ml of 0.05 M K_2PdCl_4, 11.40 ml of 0.05 M K_2PtCl_4 and 18.825 ml of 0.1 M ethylenediaminetetraacetic acid (EDTA) were added to 650 ml of ultra-pure water in a 2 liter round bottom flask. The flask was heated to 60 ^oC and kept at this temperature for 40 minutes under vigorous stirring. After 40 minutes the solution was allowed to cool to room temperature and the pH of the solution was adjusted to ca. 9-10 with a 0.3 M NaOH solution. Afterwards, 800 mg of either Vulcan XC-72 (Cabot Corporation), multi-walled carbon nanotubes (Sigma Aldrich) or reduced graphene oxide (Graphenea) was added as carbon support and this suspension was stirred for an additional 2 hours. Next, 150 ml 0.05 M Na_2CO_3 solution containing 450 mg $NaBH_4$ was added dropwise over the course of 1 hour. After this addition, the mixture was stirred at room temperature overnight. The nanoparticles were collected by centrifugation at 4500 rpm for 20 minutes, and were washed four times with ultra-pure water.

X-ray powder diffraction analysis was performed on a Philips X'pert diffractometer, equipped with an X'celerator, using Cu*K*α radiation. The data were recorded in the 2ϑ-range between 10^o and 100^o. For ICP-OES, nanoparticle samples were first allowed to dissolve in *aqua regia* (3:1 HCl/HNO_3) for at least 48h. The samples were then filtered and analyzed with a Varian Vista-MPX CCD Simultaneous ICP-OES. TEM images were obtained with a JEOL TEM 1010.

7.2.3 Electrochemical measurements

Cyclic voltammetry measurements were carried out in a standard electrochemical cell using a three-electrode assembly at room temperature. The cell and all other glassware were first cleaned by boiling in a 1:1 mixture of concentrated sulfuric and nitric acid and were cleaned before every experiment by boiling in ultra-pure

water. A highly ordered pyrolitic graphite electrode with a diameter of 5 mm was used as working electrode, on which 10 µl of a 5-wt% nafion solution containing approximately 10 mg/ml of supported $Pd_{70}Pt_{30}$ nanoparticles was dropcasted. A coiled gold wire was used as counter electrode. All potentials are reported versus the reversible hydrogen electrode (RHE) as a reference electrode in a separate compartment filled with the same electrolyte, at the same pH as the electrolyte in the electrochemical cell. The voltammograms were recorded on an Ivium A06075 potentiostat at a scan rate of 50 mV s^{-1}.

Faradaic efficiency measurements were carried out in a custom-made H-type cell with a cathodic and an anodic compartment separated by a Nafion 115 membrane (see Figure 5.1). The cell was cleaned in a similar way as the cell used for cyclic voltammetry. A pyrolitic graphite electrode with a diameter of 10 mm was used as working electrode, on which 50 µl of a 5-wt% nafion solution containing approximately 10 mg/ml of supported $Pd_{70}Pt_{30}$ nanoparticles was dropcasted. A platinum flag electrode was used as counter electrode and a Ag/AgCl reference electrode was used. The resistance of the cell was determined before every experiment by electrochemical impedance spectroscopy (EIS) on an Ivium A06075 potentiostat (see Appendix II.2). For the chronoamperometry measurements an Autolab PGSTAT101 potentiostat was used, which compensated for the ohmic drop that was measured with EIS.

7.2.4 Detection and quantification of products

For online detection of products dissolved in the electrolyte as a function of applied potential online High Performance Liquid Chromatography (HPLC) was used.[17] While changing the potential from 0.0 V to the required potential, samples were collected with an open tip positioned close (~10 µm) to the electrode. Sampling was done at a rate of 60 µL min^{-1} and each sample had a volume of 60 µL. Since the potential was changed at 1 mV s^{-1}, each sample contained the products averaged over a potential change of 60 mV. After voltammetry, these samples were analyzed by HPLC (Prominence HPLC, Shimadzu; Aminex HPX 87-H column, Biorad). Faradaic efficiencies were determined by analyzing 100 µl

aliquots of the electrolyte, which were taken every 10 minutes during electrolysis, with HPLC.

7.3 Results and discussion

7.3.1 Characterization

A previously reported nanoparticle synthesis route toward $Pd_{70}Pt_{30}$ nanoparticles was scaled up to yield approximately 1 gram of 20 wt-% $Pd_{70}Pt_{30}$ on Vulcan XC-72 (C), multi-walled carbon nanotubes (MWCNTs) and reduced graphene oxide (rGO).[14] The as-synthesized nanoparticles were characterized with X-ray powder diffraction (XRD), inductively coupled plasma optical emission spectroscopy (ICP-OES) and transmission electron microscopy (TEM). The composition of the nanoparticles could be controlled very well, even with this large scale synthesis method, showing only a slight enrichment in palladium content for the MWCNT and rGO supported nanoparticles (see Table 7.1). A slight deviation in loading was observed between the different nanoparticle samples, but all samples had an approximate loading of 20 wt-%. The XRD spectra showed peaks around 25^{o} owing to the carbon support materials and characteristic peaks for face-centered-cubic (fcc) crystalline Pd and Pt, corresponding to the (111), (200), (220) and (311) planes respectively (see Appendix IV.1, Figure AIV.1). The peak positions of the

Table 7.1 Actual compositions of the synthesized $Pt_{70}Pd_{30}$ nanoparticles and their corresponding loading on the support materials as measured with ICP-OES and their average size as measured with XRD and calculated with the Scherrer equation.

Calculated composition	Measured composition	Loading (wt%)	Particle size (nm)
$Pd_{70}Pt_{30}$/C	$Pd_{70.8}Pt_{29.2}$/C	17.1	3.8
$Pd_{70}Pt_{30}$/MWCNT	$Pd_{72.0}Pt_{28.0}$/MWCNT	19.2	3.8
$Pd_{70}Pt_{30}$/rGO	$Pd_{72.0}Pt_{28.0}$/rGO	19.7	3.8

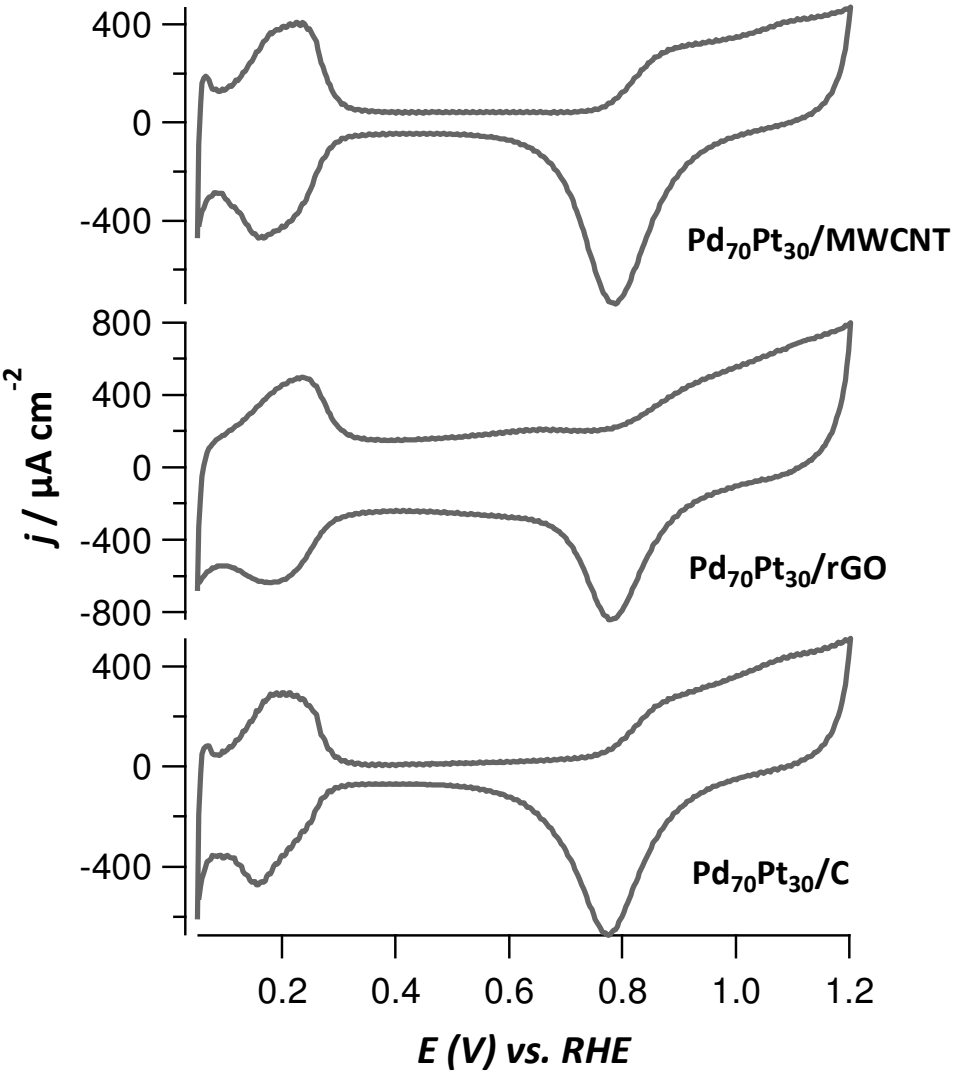

Figure 7.1 Cyclic voltammograms of the synthesized $Pd_{70}Pt_{30}$ nanoparticles on different support materials in a 0.5 M H_2SO_4 solution at a scan rate of 20 mV/s; multi-walled carbon nanotubes (MWCNT), reduced graphene oxide (rGO) and Vulcan XC-72 (C).

characteristic peaks overlapped for the XRD spectra taken with different support materials, indicating a clear similarity in nanoparticle composition. The (111) peak was used to calculate the average size of the $Pd_{70}Pt_{30}$ nanoparticles using the Scherrer equation. The average size of the nanoparticles proved to be 3.8 nm for all the samples, showing that a high degree of size control was achieved by using this synthesis route. Transmission electron microscopy (TEM) images showed that the nanoparticles were well dispersed over the support materials and that there were no large deviations in particle size (see Appendix IV.4). Particle size distributions based on the TEM images show similar average particle sizes as calculated with the Scherrer equation.

The supported nanoparticles were characterized electrochemically in a 0.5 M H_2SO_4 electrolyte by dropcasting 10 µl of a 5-wt% nafion solution containing approximately 10 mg/ml of nanoparticles on a pyrolytic graphite electrode. As can be seen in Figure 7.1, the hydrogen adsorption and desorption region, between 0.05 V vs. RHE and 0.3 V vs. RHE, shows great similarity for all samples. All voltammograms show a cathodic peak around 0.78 V vs. RHE, indicative of the stripping of oxides on the nanoparticle surface. Since this peak is reported to shift with $Pd_xPt_{(100-x)}$ composition, this further indicates that all nanoparticle samples have similar composition.[14,18]

7.3.2 Formic acid oxidation with different supports

The electro-oxidation of formic acid on $Pd_{70}Pt_{30}$ nanoparticles on different supports was studied in a 0.5 M HCOOH and 0.5 M H_2SO_4 electrolyte, with cyclic voltammograms recorded between 0.05 V and 1.0 V vs. RHE at a scan rate of 20 mV/s (see Figure 7.2). All the voltammograms show lower current densities in the forward-going scan than in the back-going scans. In the forward going scans a peak is seen around 0.3 V vs. RHE for all samples, which is correlated to the blockage of the surface by CO that is formed by formic acid dehydration.[19] Both $Pd_{70}Pt_{30}$/MWCNT and $Pd_{70}Pt_{30}$/rGO show an enhanced current density compared to $Pd_{70}Pt_{30}$/C. This is in agreement with earlier studies on single walled carbon nanotube and graphene nanosheet supported palladium nanoparticles.[20,21] With

higher potential another peak is seen around 0.9 V vs. RHE in the forward going scan which is related to the stripping of adsorbed CO. At this potential the surface of the nanoparticles starts to oxidize, thus diminishing the activity towards formic acid oxidation. In the back scan the surface oxide is stripped, leading to a subsequent increase in formic acid oxidation current densities. Major differences between the nanoparticles on different supports are seen in the back-going scan. While $Pd_{70}Pt_{30}$/C and $Pd_{70}Pt_{30}$/rGO show similar current densities, the current density of $Pd_{70}Pt_{30}$/MWCNT is significantly higher. Furthermore, a shift in the peak potentials in the back-going scan is seen. This peak in the current density is due to a renewed blockage of the surface by adsorbed CO that cannot be stripped off at these lower potentials. For $Pd_{70}Pt_{30}$/MWCNT this peak is seen around 0.6 V vs. RHE, while for $Pd_{70}Pt_{30}$/rGO and $Pd_{70}Pt_{30}$/C the peak is seen at 0.56 V vs. RHE and 0.5 V vs. RHE respectively.

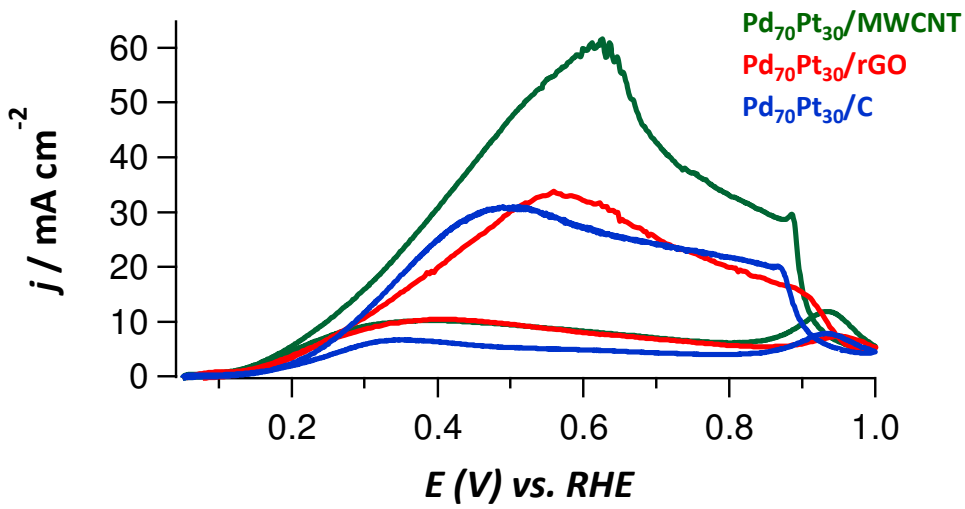

Figure 7.2 Cyclic voltammograms recorded of $Pd_{70}Pt_{30}$ nanoparticles on multi-walled carbon nanotubes (MWCNT, green), reduced graphene oxide (rGO, red) and Vulcan XC-72 (C, blue) in a 0.5 M H_2SO_4 electrolyte containing 0.5 M formic acid at a scan rate of 20 mV/s.

7.3.3 CO_2 reduction with different supports

The electrochemical reduction of CO_2 on the same nanoparticles was studied in a pH 6.7 phosphate buffer, with cyclic voltammograms recorded between 0 V and -1.5 V vs. RHE at a scan rate of 50 mV/s (see Appendix IV.5). All the nanoparticle samples show very similar behavior, with a negligible difference in current density between blank scans in which the electrolyte was purged with argon and scans with CO_2 dissolved in the electrolyte. Furthermore, the overall current densities that were observed for the nanoparticles on different supports are very similar.

The production of formic acid during CO_2 reduction in a pH 6.7 phosphate buffer electrolyte on the $Pd_{70}Pt_{30}$ nanoparticles was followed with online HPLC. In Figure 7.3 the production of formic acid is shown, normalized to the amount of nanoparticles present on the electrode. All samples show a peak in formic production; for the $Pd_{70}Pt_{30}$/C nanoparticles this peak occurs around -0.5 V vs. RHE, while for $Pd_{70}Pt_{30}$/rGO and $Pd_{70}Pt_{30}$/MWCNT it is -0.54 V vs. RHE and -0.42 V vs. RHE, respectively. The amount of formic acid produced on $Pd_{70}Pt_{30}$/C

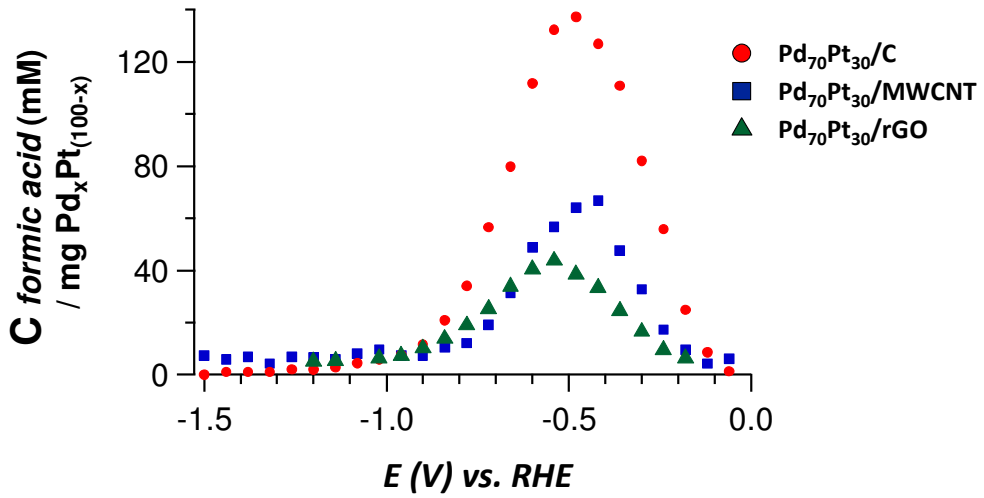

Figure 7.3 Formation of formic acid as detected by online HPLC on $Pd_{70}Pt_{30}$ nanoparticles on Vulcan XC-72 (C, ●), multi-walled carbon nanotubes (MWCNT, ■) and reduced graphene oxide (rGO, ▲) in a 0.1 M K_2HPO_4 / 0.1 M KH_2PO_4 electrolyte (pH 6.7).

nanoparticles is almost twice as high as the amount that was produced on $Pd_{70}Pt_{30}$/MWCNT, whereas the $Pd_{70}Pt_{30}$/rGO nanoparticles show the lowest amount of produced formic acid.

Figure 7.4 shows the Faradaic efficiency of CO_2 reduction to formic acid for the nanoparticles during 2 hours of electrolysis at different applied potentials. As observed previously, the $Pd_{70}Pt_{30}$/C particles show a maximum Faradaic efficiency of 91.8% after 30 minutes of electrolysis and 88% after 1 hour of electrolysis at -0.4 V vs. RHE, decreasing to 58% after two hours of electrolysis. It can be seen that the rGO supported nanoparticles show poorer efficiencies for formic acid production. The efficiency for this sample is best at an applied potential of -0.5 V vs. RHE, where a faradaic efficiency of 41% is achieved after 30 minutes of electrolysis, decreasing to 21% after 2 hours of electrolysis. Surprisingly, a maximum faradaic efficiency close to 100% after 30 minutes of electrolysis at -0.2 V vs. RHE was achieved with $Pd_{70}Pt_{30}$/MWCNT, decreasing to 64% after 2 hours.

Both the Faradaic efficiency measurements and the online HPLC measurements show that the support material has a profound effect on the electrochemical CO_2 reduction toward formic acid on these nanoparticles. The absolute amounts of formic acid that are produced are very dependent on the support material, with Vulcan supported nanoparticles outperforming both the MWCNT and rGO supported nanoparticles. The faradaic efficiencies toward formic acid however depend on the potential-dependent selectivity towards formic acid. Here, the Vulcan and MWCNT supported materials outperform the rGO supported particles, but there is a significant difference in the optimal potential for CO_2 reduction to formic acid on Vulcan supported and MWCNT supported particles.

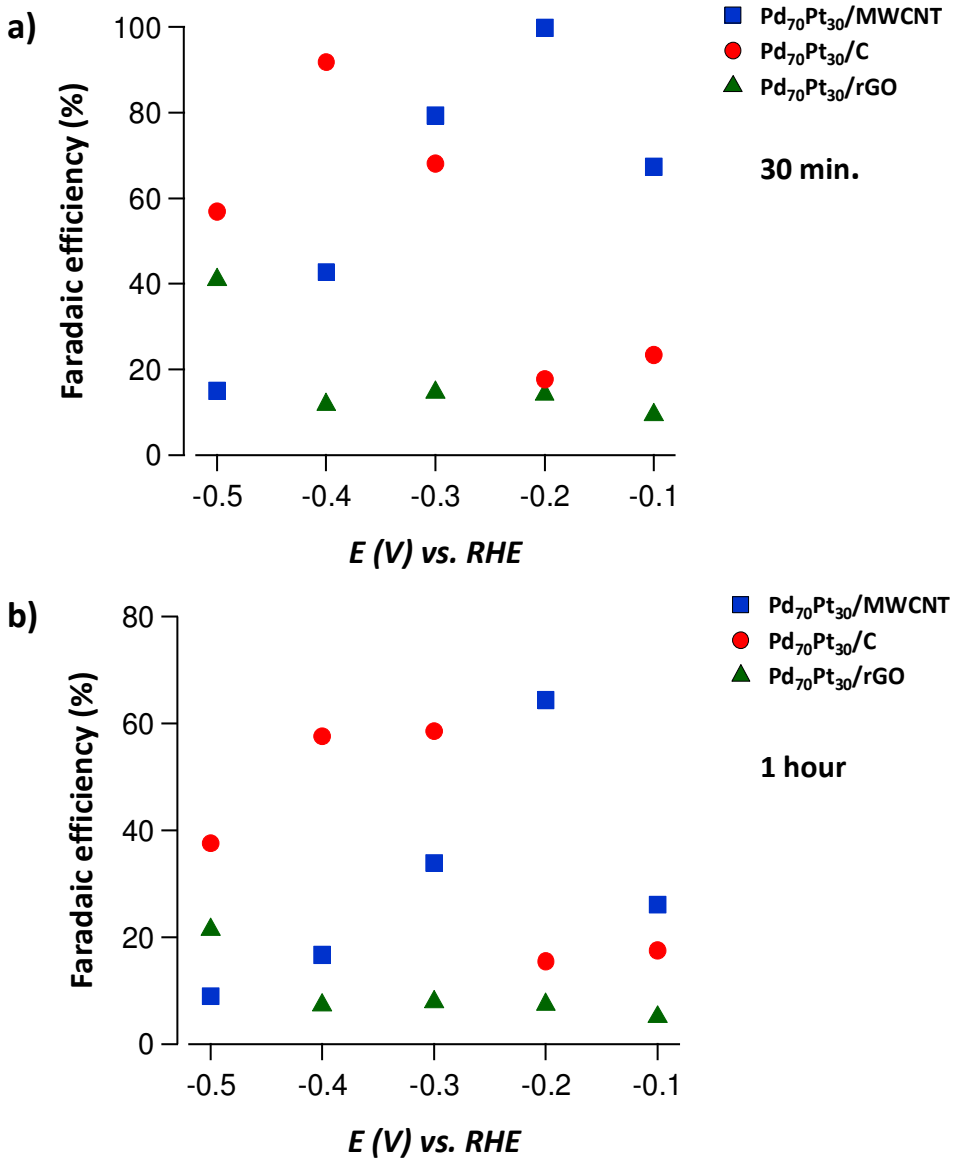

Figure 7.4 Faradaic efficiencies towards the production of formic acid on $Pd_{70}Pt_{30}$ nanoparticles on Vulcan XC-72 (C, ●), multi-walled carbon nanotubes (MWCNT, ■) and reduced graphene oxide (rGO, ▲) in a pH 6.7 phospate buffer (0.1 M KH_2PO_4/ 0.1 M K_2HPO_4) at different potentials after; **a)** 30 minutes of electrolysis; **b)** 1 hour of electrolysis.

7.4 Conclusion

We have shown that both the oxidation of formic acid as the reduction of CO_2 on $Pd_{70}Pt_{30}$ nanoparticles is strongly influenced by the support material of the particles. While $Pd_{70}Pt_{30}$/MWCNT outperforms both the rGO and Vulcan supported particles for the electro-oxidation of formic acid, both Vulcan and MWCNT supported nanoparticles perform better the rGO supported particles for the reduction of CO_2. Furthermore, a difference in the optimal applied potential is observed for CO_2 reduction on $Pd_{70}Pt_{30}$/MWCNT and $Pd_{70}Pt_{30}$/C. The MWCNT supported particles perform best at an applied potential of -0.2 V vs. RHE, achieving a Faradaic efficiency of close to 100% after 30 minutes of electrolysis, while Vulcan supported nanoparticles perform best at an applied potential of -0.4 V vs. RHE, achieving a Faradaic efficiency of 92% after 30 minutes of electrolysis.

References

(1) Y. Hori in *Modern Aspects of Electrochemistry*; Vayenas, C.; White, R.E.; Gamboa-Aldeco M.E. Eds.; Springer: New York, 2008; Vol. *42*, pp. 89-189.
(2) Whipple, D. T.; Kenis, P. J. A. *J. Phys. Chem. Lett.* **2010**, *1*, 3451.
(3) Spinner, N. S.; Vega, J. A.; Mustain, W. E. *Catal. Sci. Technol.* **2012**, *2*, 19.
(4) Sánchez-Sánchez, C. M.; Montiel, V.; Tryk, D. A.; Aldaz, A.; Fujishima, A. *Pure Appl. Chem.* **2001**, *73*, 1917.
(5) Hori, Y.; Wakebe, H.; Tsukamoto, T.; Koga, O. *Electrochim. Acta* **1994**, *39*, 1833.
(6) Kuhl, K. P.; Cave, E. R.; Abram, D. N.; Jaramillo, T. F. *Energy Environ. Sci.* **2012**, *5*, 7050.
(7) Yu, X.; Pickup, P. G. *J. Power Sources* **2008**, *182*, 124.
(8) Rice, C.; Ha, S.; Masel, R. I.; Waszczuk, P.; Wieckowski, A.; Barnard, T. *J. Power Sources* **2002**, *111*, 83.
(9) Gattrell, M.; Gupta, N.; Co, A. *Energy Convers. Manage.* **2007**, *48*, 1255.
(10) Calle-Vallejo, F.; Koper, M. T. *Angew. Chem. Int. Ed.* **2013**, *52*, 7282.
(11) Nie, X.; Esopi, M. R.; Janik, M. J.; Asthagiri, A. *Angew. Chem. Int. Ed.* **2013**, *52*, 2459.
(12) Zhang, S.; Kang, P.; Meyer, T. J. *J. Am. Chem. Soc.* **2014**, *136*, 1734.
(13) Kang, P.; Zhang, S.; Meyer, T. J.; Brookhart, M. *Angew. Chem. Int. Ed.* **2014**, *53*, 8709.
(14) Kortlever, R.; Peters, I.; Koper, S.; Koper, M. T. M. *ACS Catal.* **2015**, *5*, 3916.
(15) Rasul, S.; Anjum, D. H.; Jedidi, A.; Minenkov, Y.; Cavallo, L.; Takanabe, K. *Angew. Chem. Int. Ed.* **2015**, *54*, 2146.
(16) Kortlever, R.; Balemans, C.; Kwon, Y.; Koper, M. T. M. *Catal. Today* **2015**, *244*, 58.
(17) Hayden, B. E. *Acc. Chem. Res.* **2013**, *46*, 1858.
(18) Zhang, H.-X.; Wang, C.; Wang, J.-Y.; Zhai, J.-J.; Cai, W.-B. *J. Phys. Chem. C* **2010**, *114*, 6446.
(19) Baranova, E. A.; Miles, N.; Mercier, P. H. J.; Le Page, Y.; Patarachao, B. *Electrochim. Acta* **2010**, *55*, 8182.
(20) Bong, S.; Uhm, S.; Kim, Y.-R.; Lee, J.; Kim, H. *Electrocatal.* **2010**, *1*, 139.
(21) Morgan, R. D.; Salehi-khojin, A.; Masel, R. I. *J. Phys. Chem. C* **2011**, *115*, 19413.